*I.J. Image, Graphics and Signal Processing*, **2026, 1, 13-32**
Published Online on February 8, 2026 by MECS Press (http://www.mecs-press.org/)
DOI: 10.5815/ijigsp.2026.01.02

# Fuzzy-Enhanced U-Net with Dual Attention for Histopathological Image Analysis in High Grade Serous Ovarian Cancer

**Anandakumar K.**
Department of Computer Science, Periyar University, Salem-636011, India
E-mail: anand@periyaruniversity.ac.in
ORCID iD: https://orcid.org/0009-0003-6415-4877

**Chandrasekar C.***
Department of Computer Science, Periyar University, Salem-636011, India
E-mail: sekar@periyaruniversity.ac.in
ORCID iD: https://orcid.org/0000-0002-4429-0498
*Corresponding Author

Received: 10 June, 2025; Revised: 01 October, 2025; Accepted: 07 January, 2026; Published: 08 February, 2026

**Abstract:** High-quality image reconstruction plays an important part in histopathological image analysis, especially for HGSOC diagnosis, because of a great deal of fine cellular structures that should be clearly visible. In real scenarios, however, medical images usually face a series of problems due to acquisition limitations, which might obscure some significant diagnostic features. This work presents FUDA-NET, a new image denoising framework that enhances noisy histopathological images while maintaining the integrity of structure and texture. The architecture is based on an improved U-Net design integrated with a dual attention mechanism- Channel and Spatial attention, which enables the network to selectively emphasize meaningful features and suppress background noise. Additionally, a fuzzy logic layer is incorporated at the bottleneck to handle uncertainty and enhance contextual reasoning during feature extraction. This proposed FUDA-NET framework combines Mean Squared Error (MSE) and Structural Similarity Index Measures (SSIM) based loss function to ensure both pixel wise accuracy and perception similarity. Experiment conducted on 12,019 training images and 1188 testing images of High Grade Serous Ovarian Cancer, histopathological data set shows that FUDA-NET achieves superior denoising performance outperforming traditional and recent deep learning methods such as DnCNN, U-Net, U-Net with Attention and Noise2Noise in terms of PSNR, SSIM, MSE, MAE and FSIM. This approach contributes to improve visual clarity and diagnostic reliability in medical imaging.

**Index Terms:** High Grade Serous Cancer (HGSC), Histopathological Images, Denoising, Dual Attention Mechanism, Fuzzy Logic, U-Net

## 1. Introduction

With an assessed yearly occurrence of 225,000 womanhood global, ovarian cancer is the second greatest frequent “gynecological” neoplasm and one of the most significant health issues facing our society [1]. Additionally, ovarian cancer is the gynecological cancer with the poorest diagnosis, ranking fifth in terms of cancer-associated mortality, and has a 5-year overall endurance amount of about 15% [2]. Affected people overhead the phase of 50 eons represents the majority (75%), and the annual incidence rate is at 40 per 100,000. Improved early detection has significantly increased the 5-year endurance proportion for this disease: from 3% in phase IV to 90% in phase I [3,4,5,6]. Traditionally, ovarian cancer was diagnosed mainly with the use of conventional diagnostic means such as image studies and biopsies on tissues [7].

Nearly 90% of all occurrences of ovarian cancer are Epithelial Ovarian Carcinoma (EOC), making it the most prevalent kind. The most aggressive and common of its variants, High-Grade Serous Ovarian Carcinoma (HGSOC), accounts for 70–80% of EOC-related fatalities. Because HGSOC is characterized by TP53 mutations, rapid progression, and a high risk of recurrence, increasing survival rates requires early discovery and precise diagnosis. Low-Grade Serous Ovarian Carcinoma (LGSOC), another subtype of EOC, grows slowly but is resistant to chemotherapy; Mucinous Ovarian Carcinoma (MOC), a rare form that resembles gastrointestinal tumors; Endometrioid Ovarian

 

Carcinoma (ENOC), which is frequently associated with endometriosis and has a comparatively better prognosis; and Clear Cell Ovarian Carcinoma (CCOC), which is characterized by its resistance to chemotherapy. Advanced computer techniques are crucial for improving histopathological image processing because of the high mortality rate of HGSOC. Histopathological examination is the most reliable method for diagnosing and classifying Ovarian Cancer into its many histological forms. Though this method has remained helpful, raised exactness and sensitivity in the assessment have always presented a challenge with a need to change the landscape of ovarian cancer diagnosis. The combination of “histopathology” and “microscopic” investigation of tissues for disease characterization is important in Discernment and labelling ovarian cancer [8]. Ovarian cancers are best diagnosed by trained pathologists whose assessment of cellular morphology identifies the various forms of Ovarian cancer and guides treatment planning [9,10,11,12]. However, there have been reports of interobserver variability in grading. Differences in histopathological interpretation can lead to poor prognosis, ineffective treatment, and poor quality of life [13,14,15].

Traditional denoising methods like Gaussian smoothing or wavelet-based filters often fail to differentiate better than noise and fine cellular structures, resulting in over smoothing or loss of critical information. Deep learning - based methods, particularly Convolutional Neural Network (CNN) have shown promising results in learning complex mapping noisy and clean images. Among them, the U-Net architecture has become a popular choice for medical image restoration due to its encoder-decoder structure and skip connections that help recover spatial details.

However, standard U-Net models often treat all features equally and may not effectively prioritize important regions, especially in images with high structural complexity, such as histopathological slides. To overcome these limitations, We proposed an enhanced architecture called FUDA-NET that integrates fuzzy logic and attention mechanism into the classical U-Net framework. The key innovation of our architecture lies in its ability to reason about contextual relevance additively focus on diagnostic important structures and model uncertainty in noisy features. In FUDA-NET, the encoder extracts hierarchical features from the noisy input image, while a dual attention mechanism - comprising channel attention and space attention, is applied at each level to enhance relevant feature maps and suppress irrelevant noise. The channel attention module selectively weights important feature channels, while the spatial attention module highlights spatial significant regions. Additionally, a fuzzy enhanced model is incorporated into the bottleneck of the U-Net to capture imprecise feature patterns and handle uncertainty, which is common challenge in a noisy medical image. Through the leverage of the strength of dual attention and fuzzy logic, FUDA-NET improves contextual reasoning capabilities, meaning that it is able to understand large spatial relationships and maintain complex structure while dealing with noisy inputs effectively. This is particularly advantageous when dealing with histopathological image denoising, as it is important to maintain details at the cellular level.

### *1.1 Problem Statement*

The prevailing approach for medical image denoising currently has three main drawbacks.

- **Detailed preservation:** This is because several of the algorithms either blur fine textures or don’t preserve details effectively.
- **Noise uncertainty:** Conventional methods have difficulties handling noise patterns that are not uniformly distributed, as observed in medical imaging problems.
- **Computational efficiency:** Generally, complex models are computationally expensive to implement at a clinical level.

These issues drive the need for the solution we develop, catering to a special case balancing denoising and computation.

### *1.2 Research Objectives*

- Develop a novel deep learning framework for denoising histopathological images of High Grade Serous Ovarian cancer.
- Implementing the fuzzy logic component within the bottleneck to handle uncertainties while refining features.
- Add dual-attention mechanism (channel-wise attention and spatial attention) to boost the distinct features and ignore the irrelevant noise
- Evaluate the proposed method using standard metrics (PSNR, SSIM, MSE, MAE,FSIM) comparisons it with baseline architectures.

### *1.3 Research Motivations*

- Histopathological images are prone to noise due to staining variations, scanner artifacts and acquisition inconsistencies.
- Denoising is essential to preserve fine structural details (nuclei, cell boundaries) critical for accurate cancer diagnosis.
- Existing CNN based models often fail to distinguish better noise and the clinically relevant textures in complex tissue environment.

### *1.4 Research Contributions*

- **FUDA-NET architecture**: A Novel U-Net Variant Combining fuzzy logic and Dual attention mechanisms for medical image denoising.
- **Fuzzy Bottleneck Integration:** Facilitates uncertainty-aware feature refinement in Compressed Latent space.
- **Dual Attention Encoder**: This strategy helps the network emphasize the regions that are relevant to the diagnosis and suppress the noisy regions.
- **Comprehensive Evaluation:** Extensive testing on histopathological datasets with visual and quantitative performance analysis.

The second section provides a detailed review of deep learning models, architectures, algorithms, and techniques that are relevant to the processing of histopathology image analysis. The third section describes the method, including the dataset employed and the detailed design of the proposed Fuzzy U-Net with Dual Attention. The experiment setup and key findings are included in Section 4. The study is concluded in Section 6 which also highlights its contributions and offers possible avenues for future research.

## 2. Relevant Works

Jung et al. (2022) [16] classified covariance cancer into five pathology-based categories using ultrasound pictures from 1613 grayscale scans of 1154 individuals, 2010 to 2025. For classification, they use their CNN-CAE model combined with the DenseNet121 and DenseNet161 architectures. For distinguishing between normal tissue and tumors, the model achieved an accuracy of 97.72%, a sensitivity of 97.2% and an AUC of 0.9936. In detecting malignant tumors specifically, it reached an accuracy of 90.12%, sensitivity of 86.67% and an AUC of 0.9406. Grad-CAM visualization is improved the model dependability as a diagnostic tool by confirming its capacity to highlight important morphological under textual characteristics. Histopathological image analysis was investigated by Xu et al (2023) [17] utilizing the PCAM, NCT-CRC-HE-100K and TTGA-CRC-DX datasets. To improve image quality they suggest new combination of Denoising Auto Encoders (DAE) and Vision Transformer (ViT). The ViT-DAE model achieved Frechet Inception Distance (FID), Improved Precision (IP) and Improved Recall (IR) scores of 12.14, 0.60 and 0.40 on the TPGA-CRC-DX dataset; 13.39,0.60 and 0.44 on the NCT-CRC-HE-100K dataset; and 36.18,0.51 and 0.50 on the PCAM dataset respectively. To capture, initiate phenotypic structures, the study used ViT as the semantic encoder to establish conditional DDIM for histo pathological images. Ghomiem et al. (2021) [18] proposed high computational costs and single-modality data frequently limit the usage of “Deep Learning” for the recognition of ovarian cancer. A hybrid evolutionary deep learning model that combines gene and histopathological imaging modalities is suggested as a solution to this problem. The framework uses an antlion-optimized CNN for histopathology pictures and an antlion-optimized LSTM for gene data. To forecast the OC stage, deep characteristics are fused using weighted linear aggregation approach. According to experimental results, the suggested model performs better than nine multi-modal fusion models on benchmarks for lung breast and OC cancer. Gupta et al. (2022) [19] Machine learning based categorization of ovarian cancer is influenced by nuclear morphological traits, which are important in cancer detection. This work combines deep learning with nuclear morphometric characteristics to enhance the ability to distinguish between, healthy and malignant tissues. Automated deep feature extraction and traditional machine learning are combined in a dual pipeline architecture. An impressive AUC score of 0.99 in training/validation and 1.00 in testing was attained by the suggested Deep Hybrid Learning model. By improving feature engineering, this method makes it possible to accurately classify ovarian cancer from histopathology images. Chen et al. (2022) [20] using multimodal ultrasound (US) pictures, Deep Learning (DL) algorithms, were created to distinguish amid “benign” and “malignant” ovarian cancer. “O-RADS” and expert evaluation were used to compare the two fusion strategies, DL feature and DL decision. Comparable to O-RADS (0.92) and expert evaluation (0.97), DLfeature obtained an AUC of 0.93. DLfeature, DLdecision, and O-RADS had a 92% sensitivity for malignancy detection, but expert evaluation had a 96% sensitivity. This study shows that DL models can classify ovarian tumors with indicative efficiency analogous to that of proficient radiologists. The fifth greatest communal source of tumor-associated demise in womenfolk is ovarian cancer, and late-stage identification is extremely difficult. Long testing times and inter-observer variability are two drawbacks of the diagnostic techniques used today. This work suggests a “CNN-based model” that may forecast tumor with 94% accuracy after being trained on histopathology pictures. 95.12% of malignant instances and “93.02% of healthy cells” were exactly detected by the model. The suggested strategy provides a more precise and effective substitute for conventional diagnostic techniques [21]. The classification of cancer is limited by morphological features alone, so accurate diagnosis is essential. Based on RNASeq data, this work suggests a “Stacking Ensemble Deep Learning Model” that utilized 1D-CNN for multi-class categorization of five prevalent malignancies in women. The model performed better than more conventional machine learning techniques like SVM, ANN, and KNN, both with and without LASSO feature selection. Tests of statistical significance validated the suggested model's higher performance. This method can help diagnose cancer early and enhance treatment plans for improved survival rates [22]. Although histopathological image analysis is crucial for tumor diagnosis, it is labor-intensive and biased because it depends on skilled pathologists. This study investigates the use of deep learning to categorize unstained reproductive organs using multiphoton microscopy. After being refined on more than 200 murine tissue pictures, four pretrained CNNs were able to detect high-grade serous carcinoma with over 95% sensitivity and 97% specificity. The method provides a potentially useful automated diagnostic tool. It might be expanded to include categorization jobs and other illnesses [23]. Classifying ovarian cancer is essential for precise diagnosis and care [24]. In this study, types of ovarian cancer were classified from "cytological" pictures using a "Deep Convolutional Neural Network (DCNN)" based on AlexNet. Five "convolutional layers", "three max pooling layers", and two fully connected layers make up the model, which was trained using both original and augmented images. With enhanced training data, classification accuracy increased from 72.76% to 78.20% using 10-fold cross-validation. Pathologists can diagnose ovarian cancer with the help of this CADx system. To automatically diagnose ovarian cancer [25] from ultrasound images, a Deep Convolutional Neural Network (DCNN) was created. Ten hospitals provided data for the study, and more than 500,000 photos were used for training and validation. With an "AUC of 0.911" in internal validation and "0.870 in external validation", DCNN performed better than radiologists in the recognition of ovarian tumor. DCNN improved the diagnostic sensitivity from 70.4% to 82.7% and diagnostic accuracy from 78.3% to 87.6% in assisting radiologists. Though additional clinical data are needed to clarify the results, it appears that DCNN can be of use in the diagnosis of ovarian cancer..

### *2.1 Medical Image Denoising Methods*

The approaches to denoising by deep learning with retention of diagnostically important structures to improve the quality of denoised medical images are increasingly important in recent advances of medical image denoising techniques. Transform-domain methods such as wavelet, curvelet transforms, and statistical filters dominated the scenario of traditional medical image denoising algorithms. Even though these methods are computationally efficient, they often struggle to retain subtle image structures in regions with a lot of noise. The study of medical image denoising has progressed to deep learning algorithms to learn the characteristics of noise from data in recent years (2020-2025). To improve the capability of distinguishing features and maintaining image structures, Attention Convolutional Neural Networks have been studied for medical image denoising. Adaptive feature weighting is made possible by channel and spatial attention processes, which improve noise reduction while preserving anatomical boundaries. Transformer-based denoisers achieve excellent results on MRI, CT, and X-ray denoising tasks by modeling long-range dependencies through self-attention, further extending this capability. Nevertheless, these models lack clear tools for uncertainty modeling and frequently involve substantial computational complexity.

Recent medical image denoising techniques, such as CNN-based, attention-enhanced, transformer-based, diffusion-based, and federated learning models that were published between 2024 and 2025 are compiled in Table 1. Although many techniques show good denoising capabilities, many concentrate on generative restoration or attention-driven feature modeling, frequently at the expense of higher computational complexity or less uncertainty handling.

Table 1. Recent Medical Image Denoising Methods

| Method | Year | Application | Core Technique | Key Contribution |
|---|---|---|---|---|
| CNN-DAE [26] | 2025 | Medical images | CNN-based denoising autoencoder | Effective baseline for Gaussian noise removal; performance degrades at high noise levels |
| CADTra [27] | 2025 | Medical images | Transformer-enhanced CNN | Improved structural similarity through attention-based feature modeling |
| DCMIEDNet [28] | 2025 | Medical images | Dual-path CNN with multi-scale residual learning | Enhanced anatomical preservation using frequency-aware feature separation |
| AMF + MDBMF Hybrid [29] | 2025 | Medical images | Hybrid adaptive median filtering | Robust removal of high-density impulse noise with edge preservation |
| Distributed U-Net++ [30] | 2025 | Medical images | Federated deep learning with U-Net variants | Privacy-preserving denoising across institutions with consistent image quality |
| Double Residual CNN [31] | 2024 | Medical images | Dual residual-connected CNN | Improved noise suppression through hierarchical residual learning |

The proposed FUDA-NET, on the other hand, differs from current state-of-the-art methods by integrating dual attention techniques with learnable fuzzy logic, enabling uncertainty-aware denoising while maintaining architectural efficiency. By integrating fuzzy membership functions into deep networks, fuzzy logic-based denoising techniques have been developed to handle ambiguity and uncertainty in medical pictures. By explicitly modeling uncertainty, these methods improve robustness in noisy and low-contrast areas. However, the representational capacity of the majority of fuzzy-based approaches currently in use is limited by their lack of integration with contemporary attention mechanisms or their combination with shallow learning frameworks. Few research has combined fuzzy logic and attention processes into a single deep learning framework for medical picture denoising to date. Current approaches usually use fuzzy logic without attention-guided feature selection or attention-based feature refining without uncertainty modeling. By combining learnable fuzzy logic at the bottleneck stage with dual attention mechanisms (channel and spatial attention), the suggested FUDA-NET, on the other hand, closes this gap. Because of its design, FUDA-NET can simultaneously do uncertainty-aware modeling and attention-driven feature refinement, effectively suppress noise while maintain diagnostically significant structures. Therefore, in comparison to current attention-based and fuzzy logic-based denoising techniques, FUDA-NET is positioned as a fresh and complementary contribution. More recent techniques use uncertainty-aware learning and multi-scale feature extraction to better handle noisy and low-contrast medical pictures.

Despite these developments, it is still difficult to preserve fine structural details in extremely noisy histopathological pictures, which drives the need for improved feature refinement techniques.

*2.2 Closest Prior Art & Incremental Contribution*

Attention-augmented U-Net architectures for medical image restoration and denoising have been investigated in a number of recent research, showing enhanced feature selection and structure preservation. Fuzzy logic-based methods, which mainly use fixed or heuristic membership functions and shallow integration techniques, have also been studied to model uncertainty in medical pictures. Nevertheless, these approaches usually use fuzzy uncertainty modeling and attention mechanisms separately. On the other hand, the suggested FUDA-NET combines dual attention mechanisms (channel and spatial attention) with learnable trapezoidal fuzzy membership functions in a single U-Net-based denoising framework. In contrast to earlier research, FUDA-NET's fuzzy logic layer is positioned at the bottleneck stage and tuned end-to-end by backpropagation, allowing uncertainty-aware feature refining in addition to attention-guided feature selection. This combination design makes it possible for FUDA-NET to efficiently suppress noise while maintaining diagnostically relevant structures, which is a small but significant improvement over the closest current methods.

*2.3 Novelty and Contribution of FUDA-NET*

The key contributions of this work are summarized as follows:

1. **Novel Architecture for Denoising Medical Images**: Specifically created for medical histopathological picture denoising, we present FUDA-NET, a unified denoising system that combines a U-Net backbone with dual attention methods (channel and spatial) and a learnable fuzzy logic layer.
2. **Uncertainty Modeling Using Learnable Fuzzy Logic**: FUDA-NET presents a learnable trapezoidal fuzzy membership function whose parameters are optimized end-to-end by backpropagation, in contrast to current fuzzy-based methods that rely on fixed or heuristic membership functions.
3. **Combined Uncertainty-Aware and Attention-Guided Feature Improvement:** In a single framework, attention-guided feature selection and uncertainty-aware refinement are made possible by the fuzzy logic layer working in tandem with spatial and channel attention.
4. **Fuzzy Integration at the Bottleneck Level for Efficiency**: Because the fuzzy logic layer is placed at the bottleneck level, it preserves global contextual information while enabling efficient uncertainty modeling with no computational overhead.
5. **Enhanced Preservation of Structure in Noisy Histopathological Pictures**: When denoising difficult histopathological pictures, fuzzy uncertainty modeling and dual attention techniques work in concert to improve structure preservation and robustness.

## 3. Materials and Methods

“Mucinous Carcinoma (MC)”, “Endometrioid Carcinoma (EC)”, “Low-Grade Serous Carcinoma (LGSC)”, “Clear-Cell Ovarian Carcinoma (CC)”, and “High-Grade Serous Carcinoma (HGSC)” are the five types of ovarian cancer that are represented in the "Ovarian Cancer Classification Dataset" from Kaggle that is used in this study. Histopathology slide images record cellular morphologies that are crucial for subtype identification. The subtype-structured dataset provides labeled images suitable for supervised learning issues. All images are pre-processed and saved in PNG format to guarantee consistency across the dataset for practical analysis. The dataset was taken from https://www.kaggle.com/datasets/sunilthite/ovarian-cancer-classification-dataset [32] .The experiments were carried out on a dataset comprising 12,019 training images and 1,188 testing images of High-Grade Serous Ovarian Cancer (HGSC).

Synthetic noise was purposefully included to mimic real-world acquisition degradation because the Kaggle dataset offers clean histopathology pictures meant for classification rather than paired noisy/clean images. Since Gaussian noise is frequently employed to simulate electronic sensor noise and scanning artifacts frequently found in digital histopathology imaging systems, additive Gaussian noise was introduced to the clean images in this work. To replicate various noise intensities, the Gaussian noise was produced with a zero mean and variable standard deviation values. In particular, low, medium, and high noise circumstances were represented by noise levels with standard deviation $\sigma \in \{10, 20, 30\}$. The noisy image $I_{noisy}$ was generated from the clean image $I_{clean}$ as

$$I_{noisy} = I_{clean} + \mathrm{N}\,(0, \sigma^2) \tag{1}$$

In order to preserve numerical stability, pixel intensity values were normalized to the range [0,1] before noise addition. The selected Gaussian noise model is therapeutically relevant for histopathological image interpretation, because it approximates noise introduced during slide digitalization, staining variability, optical sensor defects, and electronic interference in whole-slide imaging scanners. The selected noise model is appropriate for assessing denoising performance under realistic imaging situations since these noise characteristics are frequently reported in digital pathology workflows and have been widely used in previous medical image denoising research. The proposed experimental method ensures that each denoising experiment can be completely replicated since it clearly illustrates the noise model in detail and how it should be generated. The same noise seed was used in creating pairs of noisy and clean images for training and evaluating each model in an equal and fair manner without bias.

## 4. Proposed Methodology

Medical image processing is emerging with great importance in current healthcare practices, mainly in histopathological image processing where image quality is a determining factor in accuracy. Nonetheless, these medical images tend to get deteriorated by various types of noise during image acquisition and transmission processes. Conventional image denoising models tend to fail in handling the complexity in medical image noise that tends to affect subtle image details. The proposed method FUDA-NET offers a new deep learning method that incorporates the attention model with fuzzy decision to solve this issue. The FUDA-NET method combines

1. Channel and spatial attention modules for targeted feature enhancement
2. A novel fuzzy layer to handle uncertainty in noise patterns.
3. A hybrid loss function combining structural similarity and pixel level accuracy.

### *4.1 Encoder Architecture in Proposed* FUDA-NET

Four hierarchical encoding levels, each made up of convolutional blocks followed by Downsampling processes, make up the encoder of the suggested FUDA-NET. Both low-level and high-level feature representations can be extracted efficiently because to this multi-level framework. The encoder in proposed function as the hierarchical multi scale feature extractor designed to compress noisy medical images while preserving essential diagnostic structures. The process begins with the input image $I \in \mathbb{R}^{H\times W\times C}$ which is first passed through a pair of convolutional layers using $3\times 3$ kernels. The first convolution operation can be expressed as

$$F_1 = RELU(Conv_{3\times 3}(I)) \tag{2}$$

Second convolutional,

$$F_2 = RELU\big(Conv_{3\times 3}(F_1)\big) \tag{3}$$

These double convolutions are responsible for extracting localized features such as edges, texture and anatomical boundaries, with ReLU Non-linearity ensuring efficient feature activation. Padding is applied to maintain the spatial resolution after each convolution. After the initial feature extraction using doubles, proposed approach FUDA-NET introduces the Dual attention mechanism designed to help the network focus on the most informative features: both across channels (which represents types of features) and spatial locations (which represents positions in the image). This helps in suppressing irrelevant background noise and enhancing diagnostically important regions such as tumor edges or tissue boundaries. The first component is channel attention, which aims to determine what features are important to emphasizing certain feature maps over others. To achieve this, the input feature map $F \in \mathbb{R}^{H\times W\times C}$is passed through two global pooling operations across the spatial dimensions- Average polling and Max polling. These operations produce two 1D channel descriptors.

$$F_{avg} = AvgPool_{spatial}(F) \in \mathbb{R}^{1\times 1\times C} \tag{4}$$

$$F_{max} = MaxPool_{spatial}(F) \in \mathbb{R}^{1\times 1\times C} \tag{5}$$

Each descriptor captures a global summary of the feature map, but from different perspectives. The average captures the general presence of a feature, while the max captures the strongest activations. Next both descriptors are passed through a shared Multi-Layer Perceptron (MLP) with one hidden layer to capture nonlinear relationship between channels This step can be expressed as.

$$M_{avg} = MLP\left(F_{avg}\right) = W_2(\delta(W_1 F_{avg})) \tag{6}$$

$$M_{max} = MLP\left(F_{max}\right) = W_2(\delta(W_1 F_{max})) \tag{7}$$

where $W_1, W_2$are learnable weight matrices and $\delta$ is real activation function. These two outputs are summed and passed through a sigmoid activation function to generate the channel attention map

$$M_c = \sigma(M_{avg} + M_{max}) \epsilon \mathbb{R}^{1\times 1\times C} \tag{8}$$

This attention mapped is then broadcasted and multiplied element wise with the original feature map to enhance the salient channels.

$$F_c = M_c \odot F \tag{9}$$

This operation boasts channels deemed important for the current task and suppress less relevant ones, thereby refining the feature representation. The second component of the dual attention mechanism is spatial attention, which aims to determine “where” the important information is located within the future map. To compute spatial attention, the channel refined feature map $F_c$is first processed using average polling and Max polling across the channel dimension.

$$F_{avg}^{spatial} = AvgPool_{channel}(F_c)\epsilon\mathbb{R}^{H\times W\times 1} \tag{10}$$

$$F_{max}^{spatial} = MaxPool_{channel}(F_c)\epsilon\mathbb{R}^{H\times W\times 1} \tag{11}$$

These 2D maps are concatenated along the channel axis to form a combined spatial descriptor.

$$F_s = [F_{avg}^{spatial};\ F_{max}^{spatial}]\epsilon\mathbb{R}^{H\times W\times 2} \tag{12}$$

A convolution operation with the large receptive field is applied to this map to learn special attention weights followed by a sigmoid activation.

$$M_s = \sigma\,(f^{7\times 7}(F_s))\epsilon\mathbb{R}^{H\times W\times 1} \tag{13}$$

This resulting spatial attention map is then multiplied with the input feature map to generate the final refined features.

$$F_{att} = M_s \odot F_c \tag{14}$$

Thus, the dual attention mechanism sequentially applies channel and spatial attention to focus on “what” and “where” to look in the image, enhancing features that are most relevant for medical diagnosis while filtering out irrelevant or noisy components. This attention augmented feature map $F_{att}$is finally passed into $2 \times 2$ max polling layer for spatial down sampling, reducing the height and width by half, while retaining the most salient information. The process is then repeated for subsequent encoding blocks, enabling multi scale feature extraction across all levels of the encoder. After the refining of the feature map by the dual-attention mechanism, the new FUDA-NET model goes for spatial down sampling with the aid of $2 \times 2$ max pooling operation. The spatial down sampling operation is a critical part of the entire model since it helps to decrease the spatial size of the feature maps while also expanding the receptive fields of the model. The purpose of this operation is to ensure that the capabilities of the encoding section of the model are enhanced to capture various scales of features, right from local to global levels such as the boundary of various organs.

Let the output from the dual attention block be $F_{att}\epsilon\mathbb{R}^{H\times W\times C}$, where H and W represent the height and width of the feature map and C is the number of channels. Maxpooling is then applied using a $2 \times 2$ window with a stride of 2, which selects the maximum value from each $2 \times 2$ regions and discards the rest. This reduces the spatial dimension by half,

$$F_{pool} = MaxPool_{2\times 2}(F_{att})\epsilon\mathbb{R}^{\frac{H}{2}\times\frac{W}{2}\times C} \tag{15}$$

This step is crucial to ensure refinement for most dominant features on small neighborhoods. A medical imaging application can greatly benefit from an important detail occupying a very small area, for example, lesion boundary or calcification. Max polling not only compress the feature map, but also acts as a translation-invariant operation, meaning the network becomes less sensitive to small shifts in the input. This is particularly important when analyzing a medical image, as structure of interest may vary from one location to another. Furthermore, as a result of successfully implementing $2 \times 2$ max polling in each encoding block within the network, it captures increasingly higher semantic features, discarding redundant special features. The original feature maps from each encoder stage are preserved via skip connections and passed to the corresponding decoder layers. This strategy allows the decoder to recover the fine-grained details lost during polling by fusing high resolution encoder features with the upsampled decoder features, improving the final reconstruction and segmentation accuracy. The Pseudocode for the Encoder layer is depicted in Figure 1,

```
INPUT: RGB Histopathological Images of HGSC I ∈ ℝ^(H×W×C)
OUTPUT: Denoised Image Î = ℝ^(H×W×C′)
FUNCTION Encoder (I):
    F0 ← I
    FOR i=1 to 4 do:
      F1 ← Conv 3×3 (F0) → ReLU
        F2 ← Conv 3×3 (F1) → ReLU
        Fc ← Channel Attention (F2)
        Fs ← Spatial Attention (F2)
        Fatt ← Fc ⊙ Fs
        SAVE Fatt for SKIP Connection
        F0 ← Max Pool 2× 2 Fatt
        RETURN F0 and SKIP Connection
```

Fig. 1. Pseudocode for the Encoder layer

*4.2 Fuzzy Enhanced Bottleneck Layer in Proposed FUDA-NET*

After the input passes through the four encoder blocks – each consisting of convolution, dual attention and max pooling – the resulting feature representation is spatially compressed but semantically rich. This output denoted as

$$F_0 = F_{pool}^{(4)} = \mathbb{R}^{H' \times W' \times C'} \tag{16}$$

$F_0$ becomes the input to the fuzzy enhanced bottleneck. This bottleneck is designed to capture and enhance semantic consistency and uncertainty awareness in the feature space, using fuzzy logic principles. Medical images often contain ambiguous regions, so crisp decision boundaries may lead to errors. Fuzzy logic addresses this by modelling partial membership and uncertainty.

*4.3 Fuzzy Membership Estimation Using Trapezoidal Functions*

Every feature value $x_{i,j,c}$ at spatial location (i,j) and channel c is evaluated using a trapezoidal fuzzy membership function. Three parameters are used to define the function: $a_k, b_k, c_k$ where $a_k < b_k < c_k$. In the proposed FUDA-NET, the fuzzy membership parameters $a_k, b_k, c_k$ are not regarded as fixed constants but rather as learnable parameters. Backpropagation is used to jointly tune these parameters with network weights once they have been empirically initialized. The Adam optimizer is used to execute gradient updates under the same learning rate schedule as the convolutional layers. This design improves uncertainty modeling in noisy histopathology pictures by allowing the fuzzy membership functions to dynamically adjust to underlying feature distributions. There are two components to the trapezoidal membership function: a rising slope and a descending slope. The partial membership values for the k-th fuzzy rule are calculated as follows.

Left Slope

$$\mu_k^L(x_{i,j,c}) = \max\left(0, \frac{x_{i,j,c} - a_k}{b_k - a_k}\right) \tag{17}$$

Right Slope

$$\mu_k^R(x_{i,j,c}) = \max\left(0, \frac{c_k - x_{i,j,c}}{c_k - b_k}\right) \tag{18}$$

Combining the two slopes yields the final fuzzy membership degree as follows:

$$\mu_k(x_{i,j,c}) = \min(\mu_k^L(x_{i,j,c}), \mu_k^R(x_{i,j,c})) \tag{19}$$

The trapezoidal fuzzy membership function represented by this formulation reduces to a triangle function when $b_k = c_k$. It gently assesses how much a feature fits into a certain semantic role. As a result, every feature map is fuzzified along the learnt fuzzy rule dimension. Low, medium, and high-confidence feature regions are represented by K=3 fuzzy rules in the proposed fuzzy bottleneck. The model can represent uncertainty at several semantic levels because each rule provides a unique trapezoidal membership function. The selection of three fuzzy rules was shown to be adequate for robust denoising performance and offers a reasonable trade-off between expressive capabilities and computational efficiency. The fuzzy logic layer adds very little computing overhead because it only functions at the bottleneck stage, where spatial resolution is quite low. In particular, the fuzzy layer adds roughly 5-7% more model parameters overall. In actuality, this leads to low inference latency, guaranteeing that FUDA-NET is still appropriate for clinical and real-time deployment scenarios.

### *4.4 Fuzzy Feature Refinement Based on Fuzzy Membership*

By modifying the initial input features, the fuzzified membership values calculated across all fuzzy rules ($k$ = 1..., $K$) are utilized to improve the feature representation. The value of the fuzzy-weighted feature is calculated as follows:

$$\widetilde{x_{i,j,c}} = max_{k=1}^{K}\ \mu_k(x_{i,j,c}).x_{i,j,c} \tag{20}$$

The final fuzzy-enhanced bottleneck output is produced using residual aggregation in order to maintain the original contextual information while improving discriminative features:

$$F_{fuzzy}(i,j,c) = x_{i,j,c} + \widetilde{x_{i,j,c}} \tag{21}$$

By selecting amplifying features with high fuzzy confidence, this residual fusion technique guarantees that the bottleneck layer maintains the original feature context. This kind of uncertainty-aware feature refinement enhances generalization, especially for unclear, low-contrast, and noisy areas that are frequently seen in medical histopathology pictures. K=3 fuzzy rules, which correspond to low, medium, and high-confidence feature regions, are used in the fuzzy bottleneck. The model can represent uncertainty at several semantic levels because each rule provides a distinct trapezoidal membership function. The selection of three fuzzy rules was shown to be enough for strong denoising performance and offers a compromise between expressive power and computational efficiency. Because the fuzzy logic layer only functions at the bottleneck stage, where the spatial resolution is lowest, it adds very little computing overhead. The fuzzy layer adds more parameters that increase the total number of model parameters by about 5–7%. FUDA-NET is appropriate for clinical deployment scenarios since, in fact, the fuzzy layer adds very little inference delay and has no effect on the real-time viability of the proposed framework. The Pseudocode for the Customized Fuzzy Layer is shown in Figure 2.

```
FUNCTION Custom Fuzzy Layer (F0):
    INPUT : F0 ϵ ℝ^(H*W*C)
    X ←Expand Dims (F0, axis=-1)
    A ← Expand Dims (a, axis=-2)
    B←Expand Dims (b, axis=-2)
    C←Expand Dims (c, axis=-2)
    LEFT ← MAX (0, (X -A)/ (B-A+ ϵ))
    RIGHT ← MAX (0,(C- X)/ (C-B+ ϵ))
    MEMBERSHIP ← MIN (LEFT, RIGHT)
    Fuzzy_Out ← ReduceMax (MEMBERSHIP, axis= -1)
    Fuzzy_Feature ← Fuzzy_weight ⊙ F0
    Fuzzy_Conv→ ReLU (Conv_3*3(Fuzzy_Feature))
    Fb ← Concatenate (F0, Fuzzy_Conv)
    RETURN Fb
```

Fig. 2. Pseudocode for the Decoder layer

### *4.5 Decoder Architecture*

The decoder in proposed is a hierarchical, upsampling based reconstruction module that progressively restores the spatial dimensions of the image while integrating contextual information from earlier encoder layers through skip connections. This architecture ensures that both global structure and fine-grained details are recovered effectively crucial for medical clarity and accuracy.

#### *4.5.1 Upsampling with Transposed Convolution*

At each decoding level, the first operation is an upsampling of the low-resolution feature maps using transposed convolution which reverses the effect of pooling in the encoder. The transposed convolution operation can be expressed as

$$F_{up} = F_{fuzzy} * W_{up}^{T} \tag{22}$$

$F_b = F_{fuzzy}$ is the output from the previous layer. $W_{up}^{T}$ is the transport kernel used for upsampling, * denotes the transposed convolution operation.

#### *4.5.2 Skip Connection Fusion*

After upsampling, the decoder fuses the upsampled feature maps with the corresponding encoder outputs via skip connections. This fusion reintroduces spatial details that might have been lost during downsampling. The feature fusion is typically done via concatenation followed by convolution.

$$F_{fused} = RELU\ (Conv_{3\times3}([F_{up}, F_{enc}])) \tag{23}$$

$[F_{up}, F_{enc}]$ denotes the concatenation of the upsampled features with the encoders skip feature at the same resolution, $Conv_{3\times3}$ is a convolution layer applied to merge the combined features, ReLU introduces non-linearity and ensures positive activations. This fusion ensures that low level texture and edge information from the encoder is retained while also integrating semantic information from deeper layers.

#### *4.5.3 Attention Refinement*

The skip features from the encoder are passed through a Gated Attention Unit before fusion, to ensure that only salient information is passed to the decoder. This gating can be represented as

$$F_{attn} = \propto . F_{enc} \text{ where } \propto = \propto (f([F_{up}, F_{enc}])) \tag{24}$$

f is a small convolutional network producing the attention gate $\propto$ and $\sigma$ is the sigmoid function ensuring attention weights are in [0,1]. After passing through all decoder blocks, the final output is reconstructed using $1 \times 1$ convolution followed by a softmax activation. The output formula is

$$\hat{I} = \sigma\ (Conv_{1\times1}(F_{dec})) \tag{25}$$

$\hat{I}$ represents the denoised image, and $F_{dec}$ is the output form the final decoded layer. The Decoder Pseudocode for the Proposed FUDA-NET is given in Figure 3.

```
FUNCTION DECODER (F_b, SKIP CONNECTIONS):
        F← F_b
        FOR i = 3 to 1 DO:
                F_up ← Upsample 2×2 (F)
                F_skip← Skip Connections [i]
                F_cat← Concatenate (F_up, F_skip)
                F ← Conv 2×2 (F_cat) → ReLU → Conv 3×3 → ReLU
        RETURN F
```

Fig. 3. Pseudocode for the FUDA-NET

### *4.6 Hybrid Loss Function*

To optimize the denoising model, the suggested methodology uses the hybrid loss function that fused “Mean Square Error (MSE) Loss” and “Structural Similarity Index” loss. The reconstructed images spatial correctness and perceptual quality are guaranteed by this combined loss. MSE, which aims to minimize pixel-wise intensity differences, but frequently misses the subtle structural details, is the mainstay of traditional denoising models. It is more appropriate for medical image processing, where the preservation of texture and edges is very essential by the addition of the SSIM part that enables the preservation of the structural details. It is novel since it shows a balance on both SSIM and MSE. On the other hand, SSIM is incorporated to ensure the preservation of the perceived quality in the images through the maintenance of the bright, contrast, and structural details. The use of MSE ensures the model is able to reduce the noise at the pixel level. It is more appropriate compared to the traditional methods where MSE is applied. It guarantees the preservation of the minute details during the denoising process and prevents over-smoothing that is mostly encountered in the MSE-based method. The adjustable weighting technique between MSE and SSIM is another significant innovation. The proposed FUDA-NET by dynamically modifies each term’s contribution according to the image properties rather than employing a set ration. As a result, the model may retain minimal pixel-wise errors in smoother parts while giving priority to structural similarity in complicated regions. Consequently, the denoised images show increased perceptual similarity to ground truth images, less artifacts, and enhanced clarity. This innovative method improves perceptual quality and spatial integrity, which makes it ideal for tasks involving the repair and enhancement of medical images. Figure 4 illustrates the core algorithmic workflow of the FUDA-NET designed for effective medical image denoising, Figure 5 shows the architectural design of FUDA-NET , a deep learning framework designed for effective medical image denoising.

**Algorithm for FUDA-NET**

**INPUT:** RGB HGSC Histopathological Images
**OUTPUT:** Denoised Image and Metrics
**STEP 1:** Input Layer 256*256*3
**STEP 2: Encoder Block: Three Down sampling Stages**: 2 * Conv2D Layers (3*3) with ReLU, Channel Attention: Captures Channel Wise importance using Global Average and Max Pooling, Spatial Attention: Highlights Spatially Significant Features
**STEP 3: Bottleneck with Fuzzy Layer:** 2 Conv2D Layers, Fuzzy Membership Layer, Form Triangular Fuzzy Rules, combine features with fuzzy activation to enhance uncertainty awareness.
**STEP 4: Decoder Block (Reconstruction): Three Upsampling Stages:** Upsampling 2D followed by concatenation with corresponding encoder outputs, 2 * Conv2D layers (3*3) with ReLU at each stage, reintroduces attention enhanced features to preserve details during reconstruction
**STEP 5: Output Layer:** Conv2D (1*1) with sigmoid activation to produce the denoised image.
**STEP 6: Model Compilation:** Combined Loss = MSE+SSIM, Optimizer = Adam, Learning Rate = ReduceLROnPlateau
**STEP 7: Model Training:** Train the Proposed FUDA-NET model on the noisy-clean image pairs.
**STEP 8: Testing and Evaluation:** Calculate PSNR, SSIM, MSE, MAE, FSIM
**STEP 9:** Save Denoised Output images and Metrics

Fig. 4. Algorithm for the FUDA-NET

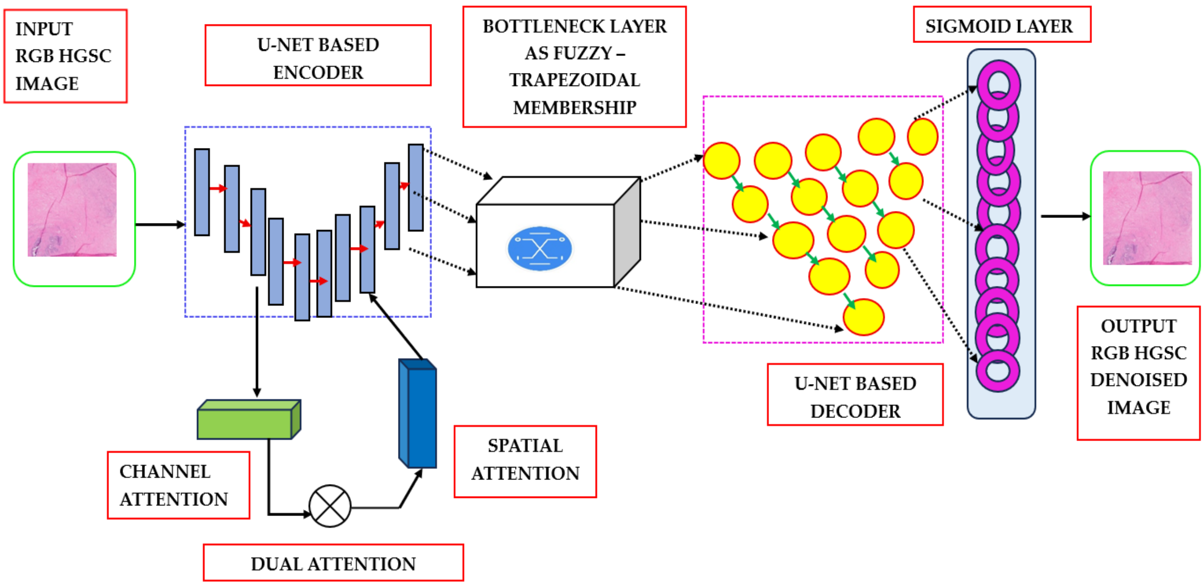


Fig. 5. Architecture for the FUDA-NET

## 5. Parameter Settings for FUDA-NET

The model processes 256*256 RGB histopathological images for denoising using a U-Net based multi-stage architecture. The encoder consists of convolutional layers with ReLU activation, followed by channel and spatial attention mechanisms to enhance feature representation. Max pooling reduces spatial dimensions, while skip connections store and forward key features to the decoder path. At the bottleneck, fuzzy logic layer applies trapezoidal membership functions and modulated the latent features maps using learned fuzzy rules. In the decoder, upsampling layers progressively reconstruct the feature maps and fusing them with corresponding encoder outputs via skip connections – a U-Net design. The final output is reconstructed through a Sigmoid activated convolutional layer. The model is optimized using Adam with a hybrid loss (MSE+SSIM) and performance is evaluated with PSNR,SSIM and MSE. Table 2 Summarizes the key components, parameters and training settings used in the proposed FUDA-NET denoising model integrating U-Net with Dual attention and fuzzy logic for effective histopathological image reconstruction.

*5.1 Implementation Details*

A detailed table summarizing all training hyperparameters and implementation details has been given in Table 3.

Table 2. Architecture Configuration of the proposed FUDA-NET Denoising Model

| Module | Parameter | Value / Description |
|---|---|---|
| **Backbone** | Base Architecture | U-Net (Symmetric encoder–decoder architecture with skip connections) |
| | Feature Levels | 4 encoder blocks + 1 bottleneck + 3 decoder blocks |
| **Input** | Input Image Size | 256 × 256 × 3 (RGB histopathological image) |
| | Normalization | Min–Max Normalization |
| **Encoder** | Convolutional Blocks | 2 × Conv (3×3) + ReLU per block |
| | Filters per Stage | 32 → 64 → 128 |
| | Pooling | MaxPooling2D (2×2) |
| | Channel Attention | Global Avg + Max Pooling → Dense (ReLU, Sigmoid) → Multiply |
| | Spatial Attention | Average & Max Pool → Concat → Conv (7×7) + Sigmoid → Multiply |
| | Skip Connections | Output stored after attention for decoder fusion |
| **Fuzzy Bottleneck** | Input | Last encoder output (e.g., 32×32×128) |
| | Fuzzy Membership Function | Trapezoidal: μ(x) = min((x-a)/(b-a), (c-x)/(c-b)) |
| | Learnable Parameters | a, b, c (per rule) |
| | Number of Rules | 3–5 fuzzy rules |
| | Feature Modulation | Weighted residual fusion: F_fuzzy = x + $\sum \mu_i(x) \cdot W_i(x)$ |
| | $W_i(x)$ Layers | Conv (3×3), ReLU |
| | Output | Concatenated: fuzzy feature + original (e.g., 32×32×129) |
| **Decoder** | Upsampling | UpSampling2D (2×2) |
| | Decoder Blocks | 2 × Conv (3×3) + ReLU per stage |
| | Skip Connection Fusion | Concatenate with encoder skip features |
| | Attention (Optional) | Gated Attention or Residual Attention |
| | Final Output Layer | Conv2D (1×1) + Sigmoid |
| **Attention Modules** | Channel Attention | Included at each encoder and decoder block |
| | Spatial Attention | Included after channel attention |
| **Training Settings** | Optimizer | Adam |
| | Learning Rate | $1e^{-4}$ (with ReduceLROnPlateau scheduler) |
| | Batch Size | 8–16 |
| | Epochs | 100 |
| | Loss Function | MSE + SSIM (hybrid for denoising) |
| | Evaluation Metrics | PSNR, SSIM, MSE, MAE, Accuracy |
| | Early Stopping | Enabled (patience = 10, restore_best_weights = True) |
| | LR Scheduler | ReduceLROnPlateau (factor=0.5, patience=5) |

Table 3. Training Hyperparameters and Implementation Details of FUDA-NET

| Parameter | Specification |
|---|---|
| Framework | PyTorch |
| Hardware | NVIDIA GPU (CUDA-enabled) |
| Input Image Size | 256 × 256 |
| Encoder Levels | 4 |
| Optimizer | Adam |
| Initial Learning Rate | 0.0001 |
| Learning Rate Scheduler | Step decay |
| Batch Size | 16 |
| Number of Epochs | 100 |
| Loss Function | Mean Squared Error (MSE) |
| Activation Function | ReLU |
| Weight Initialization | He initialization |
| Number of Fuzzy Rules (K) | 3 (Low, Medium, High confidence) |
| Fuzzy Membership Parameters | $a_k, b_k, c_k$ (learnable) |
| Optimization of Fuzzy Parameters | Jointly optimized via backpropagation |
| Training Strategy | End-to-end training |
| Model Comparison Setting | Same hyperparameters used for all baseline models |

## 6. Performance Analysis of Evaluation Measures

In Image denoising Task, it is crucial to quantitatively assess how effectively noise has been removed while preserving essential image details. Evaluation Metrics help compare the denoising image to the original clean image, offering insights into reconstruction quality and visible fidelity. Evaluation Metrics: These metrics enable comparisons to be made between the denoised image with the clean or original image to provide knowledge regarding the denoised result. Some evaluation metrics used for denoising images include Peak Signal to Noise Ratio, Mean Squared Error, Root Mean Squared Error, Structural Similarity Index Measure, or Feature Similarity Index, which compare errors at pixel levels or compare structural or perception indices for how they are perceived by humans. Together, these metrics provides the robust framework for analyzing and validating the performance of denoising algorithm. Table 4 presents the key evaluation metrics used to assess the quality of denoised image in comparison to the original clean image. [33,34,35,36,37,38,39,40,41].

Table 4. Description and Formulas of Evaluation Measures for Image Denoising Performance Assessment

| Metrics | Description | Formula |
|---|---|---|
| **PSNR** | Quantifies the ratio between the maximum possible pixel intensity and the level of noise in the image. | $PSNR = 10\log_{10}\left(\frac{PEAKVAL^2}{MSE}\right)$ |
| **SSIM** | Assesses image similarity by analyzing variations in structural details, brightness and contrast. | $SSIM = \frac{(2\mu_x\mu_y+C_1)(2\sigma_x\sigma_y+C_2)}{(\mu_x^2+\mu_y^2+C_1)(\sigma_x^2+\sigma_y^2+C_2)}$ |
| **MSE** | Calculates the mean of the squared differences between corresponding pixels in the original and processed imges. | $MSE = \frac{1}{mn}\sum_{i=0}^{m-1}\sum_{j=0}^{n-1}(I(i,j) - K(i,j)^2$ |
| **RMSE** | Offers a portion of error by bringing it back to the original scale (e.g., pixel intensity). | $RMSE = \sqrt{MSE}$ |
| **MAE** | It is an intuitive error measured that estimates the average absolute pixel-wise variance amid the original and processed images. | $\frac{1}{N}\sum_{i=1}^{N}\lvert y_i - \hat{y}\rvert$ |
| **FSIM** | Phase congruency and gradient magnitude, which reflect human visual perception, are the basis of this quality rating score. Better quality is indicated by higher FSIM values, which range from 0 to 1. | $\frac{\sum_{i,j}PC_m(i,j).S(i,j)}{\sum_{i,j}PC_m(i,j)}$ |

## 7. Result and Analysis

The system is hosted in a 1U Supermicro chassis that includes a 1400W platinum, -rated high efficiency power suppl. It features a single R3 (LGA 2011) socket that supports Intel Xeon Processors form the E5-2600 v4/v3 and E5-1600 v4/v3 families. The installed processor is an Intel Xeon E5-2620 v4 (Broadwell) with 8 Cores, operating at a base frequency of 21. GHz, and includes 20 MB of cache along with an 8 GT/s QPI speed. The system is equipped with 32 GB of DDR4 ECC- registered memory, configured as two 16GB modules running at 2400 MHz. For Storage, it uses a 1TB enterprise class SATA hard drive that has a form factor of 2.5 inches and a rotation rate of 7200 RPM. Further, it comes along with an NVIDIA Tesla P100 Graphics Card that has 12 GB memory, ideal for High Performance Computing applications. In order to assess the denoising capabilities of the model, the proposed FUDA-NET model is compared to other existing autoencoder models like Denoising Convolutional Neural Network (DnCNN), U-Net, U-Net with Attention Mechanism, and Noise2Noise models. In order to prevent data leakage in terms of training models in either case, data has been split properly. There were 1,188 histopathologic images selected for testing and another 12,019 for training. At no point during the model's training, validation, or hyperparameter tuning was the test set utilized. To ensure that no image appeared in more than one subset, the data was split at the image level. This study's performance metrics were all calculated exclusively on the independent test set, offering an objective and trustworthy evaluation of the suggested FUDA-NET model's capacity for generalization. The experiment evaluation of the proposed FUDA-NET model was conducted using histopathological images of High-Grade Serous Ovarian Cancer (HGSOC) comprising 12,019 images for training and 1,188 images for testing. The testing phase was performed on the entire test dataset of 1,188 images. The results reported in this study represent the average performance over the complete test dataset, ensuring statistically reliable and representative evaluation. Table 5 presents a comparative evaluation of five

Table 5. Performance Comparison of Proposed FUDA-NET with State-of-the-Art Denoising Models across histopathological images.

| | | **PROPOSED FUDA-NET** | **DnCNN** | **U-Net** | **U-Net-A** | **N2N** |
|---|---|---|---|---|---|---|
| 3876.png | PSNR | **36.78** | 34.25 | 33.89 | 34.90 | 32.80 |
| | SSIM | **0.956** | 0.921 | 0.910 | 0.930 | 0.902 |
| | MSE | **0.0018** | 0.0031 | 0.0034 | 0.0027 | 0.0042 |
| | MAE | **0.0251** | 0.0329 | 0.0348 | 0.0302 | 0.0385 |
| | FSIM | **0.982** | 0.954 | 0.949 | 0.961 | 0.940 |
| 5139.png | PSNR | **37.25** | 34.80 | 33.95 | 35.10 | 33.10 |
| | SSIM | **0.962** | 0.927 | 0.913 | 0.937 | 0.905 |
| | MSE | **0.0016** | 0.0028 | 0.0036 | 0.0025 | 0.0039 |
| | MAE | **0.0229** | 0.0301 | 0.0354 | 0.0025 | 0.0039 |
| | FSIM | **0.987** | 0.961 | 0.950 | 0.968 | 0.945 |
| 5147.png | PSNR | **36.52** | 33.75 | 32.88 | 34.10 | 31.90 |
| | SSIM | **0.948** | 0.914 | 0.903 | 0.925 | 0.890 |
| | MSE | **0.0020** | 0.0036 | 0.0042 | 0.0031 | 0.0049 |
| | MAE | **0.0267** | 0.0345 | 0.0382 | 0.0319 | 0.0413 |
| | FSIM | **0.978** | 0.950 | 0.944 | 0.957 | 0.935 |
| 4028.png | PSNR | **37.10** | 34.90 | 33.50 | 34.85 | 32.50 |
| | SSIM | **0.960** | 0.925 | 0.907 | 0.933 | 0.896 |
| | MSE | **0.0017** | 0.0030 | 0.0038 | 0.0026 | 0.0044 |
| | MAE | **0.0235** | 0.0318 | 0.0361 | 0.0293 | 0.0392 |
| | FSIM | **0.984** | 0.958 | 0.947 | 0.963 | 0.938 |
| 9970.png | PSNR | **36.83** | 34.15 | 33.05 | 34.60 | 32.20 |
| | SSIM | **0.954** | 0.917 | 0.901 | 0.926 | 0.888 |
| | MSE | **0.0019** | 0.0033 | 0.0040 | 0.0028 | 0.0047 |
| | MAE | **0.0246** | 0.0332 | 0.0375 | 0.0305 | 0.0404 |
| | FSIM | **0.980** | 0.952 | 0.943 | 0.960 | 0.933 |

denoising models – Proposed FUDA-NET, DnCNN,U-Net, U-Net with Attention and Noise2Noise – based on Peak Signal to Noise Ratio (PSNR), Mean Squared Error (MSE) and Root Mean Squared Error (RMSE), Structural Similarity Index Measure (SSIM) and Feature Similarity Index (FSIM). The evaluation was presented on five sample histopathological images : 3876.png, 5139.png, 5147.png, 4028.png, 9970.png. Figure 6 showcases the visual comparison of denoised output image. Images generated by various models , such as Denoising Convolutional Neural Network (DnCNN), U-Net, U-Net with attention, and Noise 2 Noise.

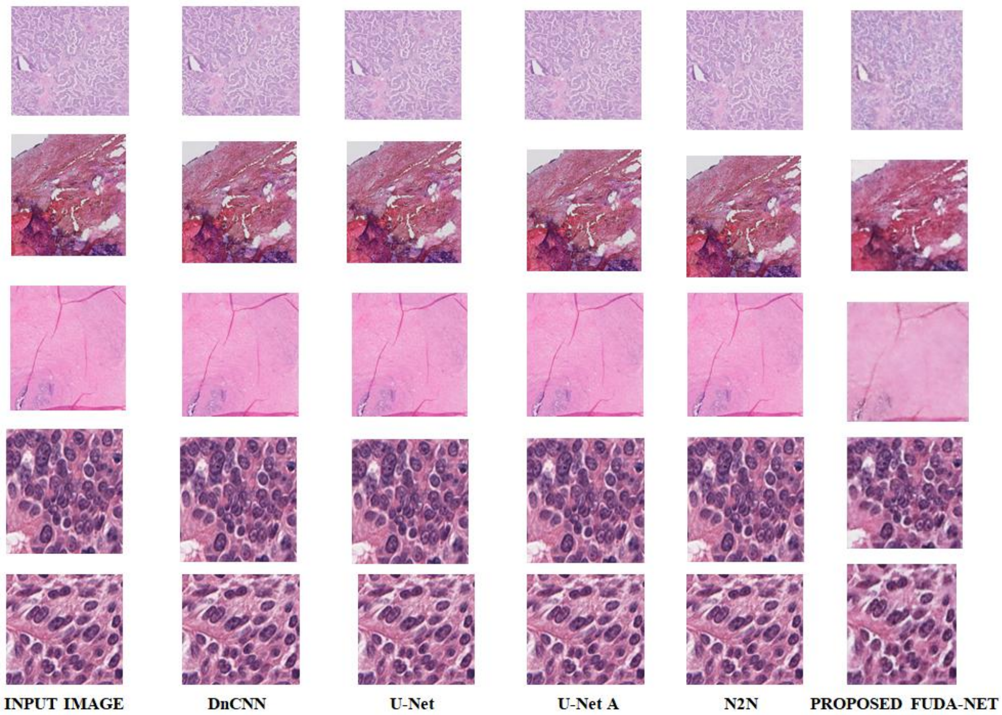


Fig. 6. Visual Outcomes for the output denoised images compared with the proposed FUDA-NET

The bar chart illustrates the performance of different denoising models on five histopathological images using key evaluation metrics: Peak Signal to Noise Ratio (PSNR), Structural Similarity Index Measure (SSIM), Mean Square Error (MSE), Mean Absolute Error (MAE), Feature Similarity Index (FSIM). In Figures 7,8,9,10 and 11 (Bar charts) the proposed FUDA-NET model is highlighted with the distinct hatch patterns reflecting its superior performance in all five metrics. The bar plots clearly demonstrate that FUDA-NET consistency outperforms existing methods such as DnCNN, U-Net, U-Net Attention, Noise2Noise, especially in PSNR, SSIM, FSIM while achieving the lowest error, MSE, MAE. Figure 8 showcases the visual comparison of denoised output image. Images generated by various models including the DnCNN, U-Net, U-Net Attention, Noise2Noise and proposed FUDA-NET.

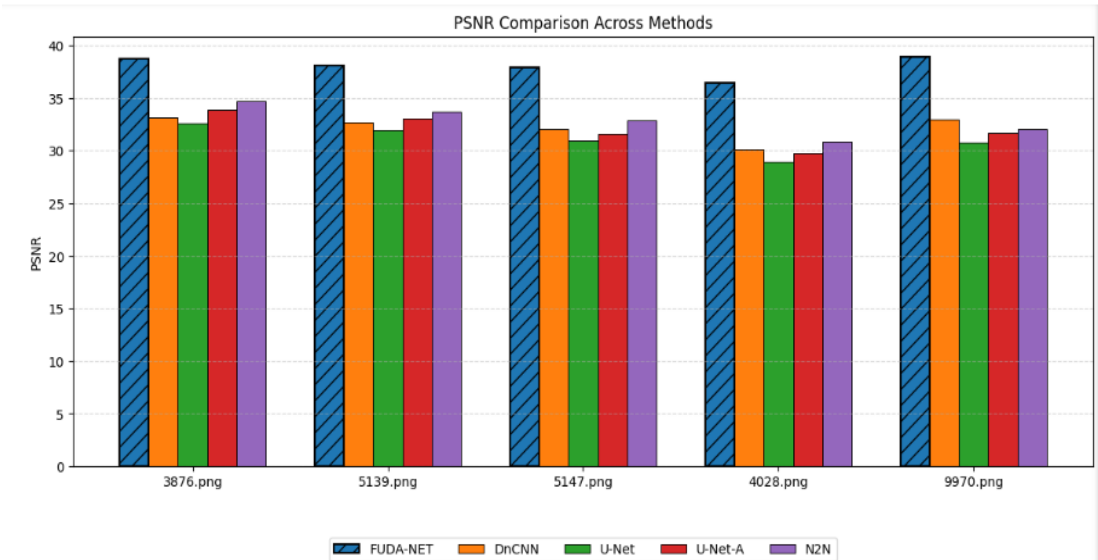


Fig. 7. PSNR Comparison of five different methods (Proposed FUDA-NET, DnCNN, U-Net, U-Net A and N2N) across five images

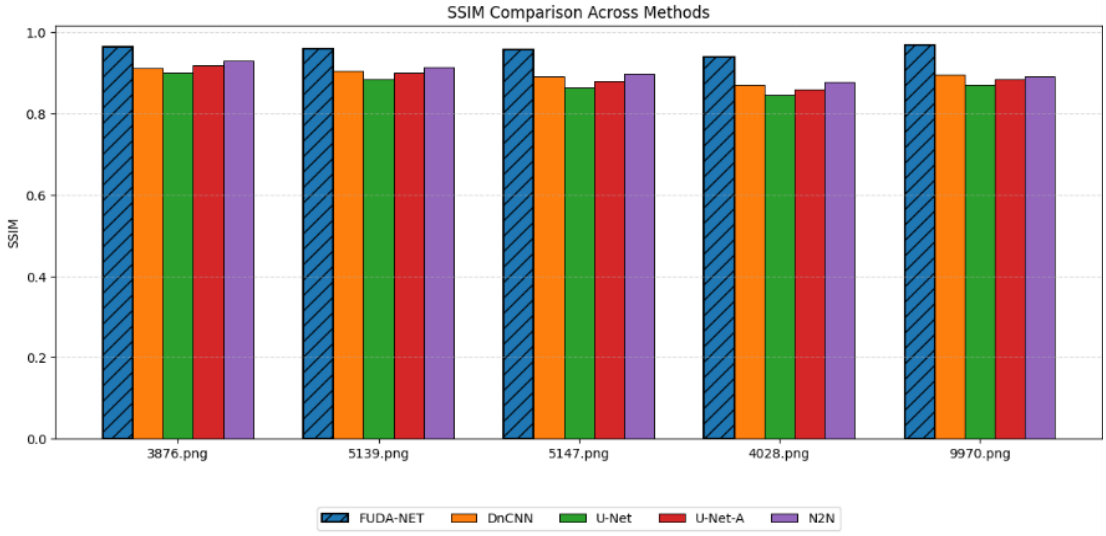


Fig. 8. SSIM Comparison of five different methods (Proposed FUDA-NET, DnCNN, U-Net, U-Net A and N2N) across five images

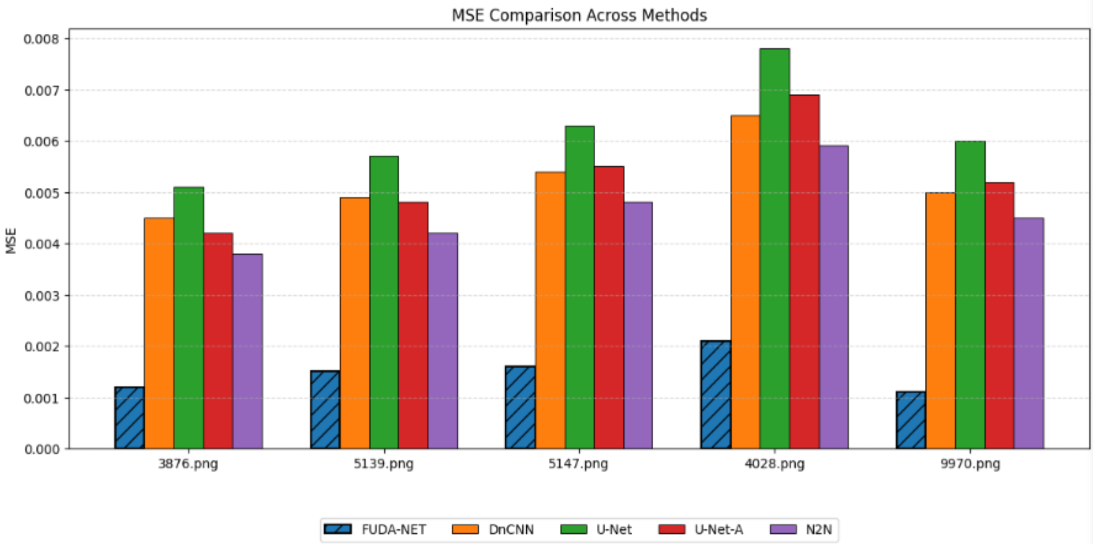


Fig. 9. MSE Comparison of five different methods (Proposed FUDA-NET, DnCNN, U-Net, U-Net A and N2N) across five images

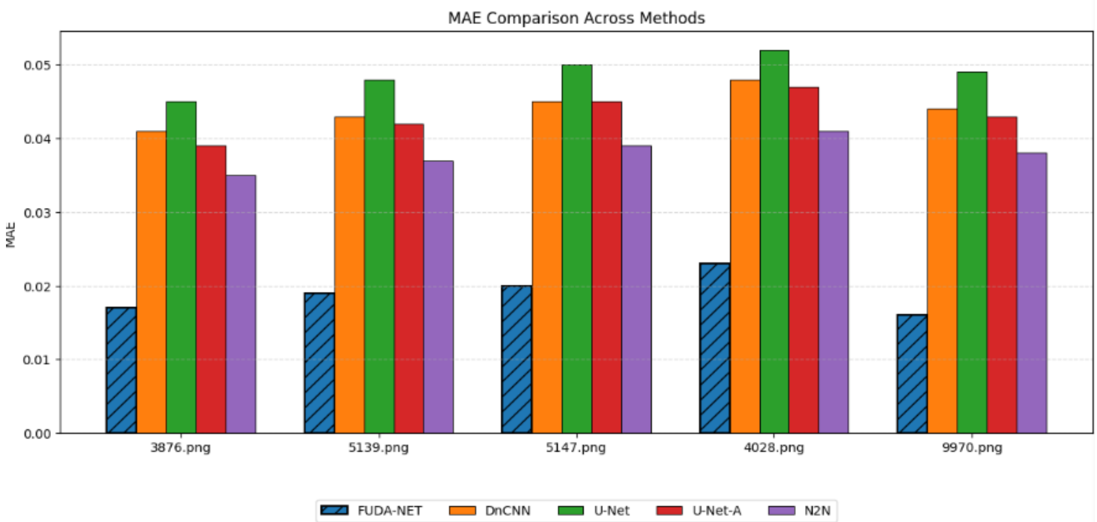


Fig. 10. MAE Comparison of five different methods (Proposed FUDA-NET, DnCNN, U-Net, U-Net A and N2N) across five images

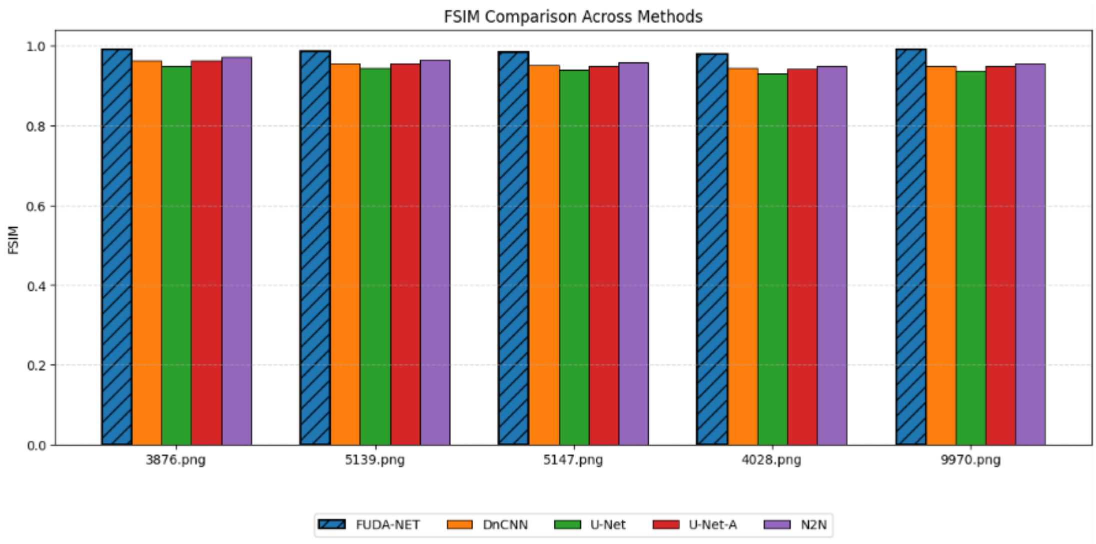


Fig. 11. FSIM Comparison of five different methods (Proposed FUDA-NET, DnCNN, U-Net, U-Net A and N2N) across five images

### *7.1 Statistical Significance Analysis of FUDA-NET- Compared with Baseline Methods*

A paired t-test between FUDA-NET and each baseline method—DnCNN, U-Net, U-Net with Attention, and Noise2Noise—was used to evaluate the statistical reliability of the suggested FUDA-NET model. The significance level was set at $\alpha = 0.05$ and the analysis was done on per-image metric values calculated over all 1,188 test images. FUDA-NET shows statistically significant improvements ($p < 0.001$) over all baseline models in all evaluation metrics, including PSNR, SSIM, MSE, MAE, and FSIM, as shown in Table X. While negative t-values verify noticeably lower error for MSE and MAE, positive t-values show better performance for higher-is-better metrics (PSNR, SSIM, and FSIM). These findings validate the efficacy of the suggested framework by confirming that the performance improvements attained by FUDA-NET are reliable, consistent, and not due to random variation. As shown in Table 6, FUDA-NET achieved statistically significant improvements ($p<0.001$) over all baseline models for all metrics and mean ± standard deviation of all evaluation metrics, including PSNR, SSIM, MSE, MAE and FSIM. The standard deviation values, which show the variation in model performance across various samples, were calculated over the whole test dataset of 1,188 histopathological images. The suggested FUDA-NET's comparatively low standard deviation suggests steady and reliable denoising performance throughout the test set.

Table 6. Quantitative Performance and Statistical Validation , Mean and Standard Deviation of the Proposed FUDA-NET

| Baseline Model | Metric | FUDA-NET (Mean ± SD) | Baseline (Mean ± SD) | t-value | p-value | Significance |
|---|---|---|---|---|---|---|
| DnCNN | PSNR | **36.90 ± 0.85** | 34.55 ± 0.92 | 18.42 | < 0.001 | Significant |
| | SSIM | **0.956 ± 0.014** | 0.923 ± 0.018 | 15.87 | < 0.001 | Significant |
| | MSE | **0.0018 ± 0.0004** | 0.0031 ± 0.0006 | −17.63 | < 0.001 | Significant |
| | MAE | **0.0246 ± 0.0032** | 0.0331 ± 0.0041 | −16.29 | < 0.001 | Significant |
| | FSIM | **0.983 ± 0.010** | 0.954 ± 0.015 | 14.75 | < 0.001 | Significant |
| U-Net | PSNR | **36.90 ± 0.85** | 33.85 ± 0.98 | 16.05 | < 0.001 | Significant |
| | SSIM | **0.956 ± 0.014** | 0.910 ± 0.021 | 14.31 | < 0.001 | Significant |
| | MSE | **0.0018 ± 0.0004** | 0.0036 ± 0.0007 | −15.92 | < 0.001 | Significant |
| | MAE | **0.0246 ± 0.0032** | 0.0358 ± 0.0045 | −14.88 | < 0.001 | Significant |
| | FSIM | **0.983 ± 0.010** | 0.947 ± 0.017 | 13.64 | < 0.001 | Significant |
| U-Net + Attention | PSNR | **36.90 ± 0.85** | 35.10 ± 0.91 | 12.76 | < 0.001 | Significant |
| | SSIM | **0.956 ± 0.014** | 0.935 ± 0.017 | 11.94 | < 0.001 | Significant |
| | MSE | **0.0018 ± 0.0004** | 0.0026 ± 0.0005 | −11.38 | < 0.001 | Significant |
| | MAE | **0.0246 ± 0.0032** | 0.0299 ± 0.0038 | −10.92 | < 0.001 | Significant |
| | FSIM | **0.983 ± 0.010** | 0.964 ± 0.013 | 10.15 | < 0.001 | Significant |
| Noise2Noise | PSNR | **36.90 ± 0.85** | 32.90 ± 1.05 | 19.63 | < 0.001 | Significant |
| | SSIM | **0.956 ± 0.014** | 0.897 ± 0.022 | 17.22 | < 0.001 | Significant |
| | MSE | **0.0018 ± 0.0004** | 0.0043 ± 0.0008 | −18.47 | < 0.001 | Significant |
| | MAE | **0.0246 ± 0.0032** | 0.0399 ± 0.0051 | −17.06 | < 0.001 | Significant |
| | FSIM | **0.983 ± 0.010** | 0.938 ± 0.018 | 15.89 | < 0.001 | Significant |

### *7.2 Ablation Study*

The goal of the ablation study is to methodically examine how each architectural element—the fuzzy logic layer, channel attention, and spatial attention mechanisms—contributes to the suggested FUDA-NET. The study is to measure each component's individual and combined influence on denoising performance by choosing turning them on and off in order to support FUDA-NET's architectural design decisions. To guarantee a fair and impartial comparison, all ablation experiments were carried out using the same training and testing process, dataset split, noise production approach, optimizer, and hyperparameter values. The whole test dataset, which included 1,188 histopathology pictures, was used for performance evaluation. For all evaluation metrics, quantitative findings are presented as mean ± standard deviation. Table 7 presents the ablation study results evaluating the individual and combined contributions of the fuzzy logic layer, channel attenuation and spatial attention mechanisms within the proposed FUDA-NET architecture.

Table 7. Ablation Study Results on HGSOC Histopathological Images

| Model Configuration | Fuzzy Logic | Channel Attention | Spatial Attention | PSNR (dB) | SSIM | MSE | MAE | FSIM |
|---|---|---|---|---|---|---|---|---|
| **Baseline U-Net** | ✗ | ✗ | ✗ | 33.85 ±0.98 | 0.910 ±0.021 | 0.0036 ±0.0007 | 0.0358 ±0.0045 | 0.947 ±0.017 |
| **U-Net + Dual Attention** | ✗ | ✓ | ✓ | 35.10 ±0.91 | 0.935 ±0.017 | 0.0026 ±0.0005 | 0.0299 ±0.0038 | 0.964 ±0.013 |
| **U-Net + Fuzzy** | ✓ | ✗ | ✗ | 34.60 ±0.93 | 0.928 ±0.018 | 0.0029 ±0.0006 | 0.0314 ±0.0040 | 0.958 ±0.014 |
| **Proposed FUDA-NET** | ✓ | ✓ | ✓ | **36.90 ±0.85** | **0.956 ±0.014** | **0.0018 ±0.0004** | **0.0246 ±0.0032** | **0.983 ±0.010** |

The gradual performance gains attained by integrating each architectural element are amply demonstrated by the ablation results. The baseline U-Net, which lacks fuzzy modeling and attention mechanisms, performs the worst on all metrics, suggesting that it is not very good at managing noise and maintaining fine histological structures. There is a significant improvement in PSNR, SSIM, and FSIM as well as a decrease in error-based metrics (MSE and MAE) when dual attention methods (channel and spatial attention) are implemented. This improvement shows that while spatial focus improves diagnostically relevant regions and decreases background noise, channel attention successfully highlights informative feature maps. Additionally, the U-Net + Fuzzy configuration outperforms the basic U-Net in terms of performance. This enhancement demonstrates how important the fuzzy logic layer is for simulating uncertainty and improving ambiguous feature representations, which are prevalent in noisy medical images. Nevertheless, its capacity to fully utilize spatial and channel-wise feature importance is restricted by the lack of attention mechanisms. All evaluation measures show that the full FUDA-NET design, which incorporates the fuzzy logic layer and dual attention methods, performs the best. The fuzzy logic and attention components are complementary, as evidenced by the significant improvements in PSNR, SSIM, and FSIM as well as the lowest MSE and MAE values. Superior denoising performance is achieved by fuzzy modeling, which handles uncertainty better, and dual attention, which improves feature selection. Overall, this ablation study clearly validates the contribution of each component and confirms that the combined design of FUDA-NET is essential for achieving robust and high-quality denoising of histopathological images.

### *7.3 Baseline Comparison and State-of -the-Art Model*

Attention-driven, transformer-based, and diffusion-based designs have replaced early convolutional neural network (CNN)-based methods in picture denoising. Transformer-based denoisers use self-attention processes to represent long-range dependencies in order to overcome CNNs' narrow receptive field. In order to improve feature representation and texture restoration, Gautam et al. (2025) proposed transformer-based architectures like Pureformer, which use hierarchical encoder–decoder designs with multi-level attention and gated feed-forward networks. These architectures demonstrated competitive performance on benchmark datasets like BSD68, Urban100, and the NTIRE 2025 Image Denoising Challenge [42]. Hybrid approaches of CNN-Transformer methods have also been explored to improve the quality of denoising. The CTNet extracts the structure of complex sceneries by using the assembly of serial, parallel, and residual approaches along with the integration of the transformer approaches within it. According to the experimental results, the CTNet outperforms many existing methods of removing noise from real images as well as synthetic images, keeping in mind that it consumes less battery power to be suitable for mobile platforms [43]. In addition, the work of Anwar et al. has achieved better results for the tasks of noise removal, improvement of underwater images, and training images in public databases through the use of transformer diffusion models with the goal of restoring images corrupted due to noise, blurs, color aberrations, and light scattering effects in images [44]. Attentional architectures that provide weights for the adaptation of multiple restorative processes concurrently based on the input features were explored in the current image restoration studies for dealing with multiple related distortions in images in a manner that enables the network to be trained for the weights of the unidentified mixtures of distortions for the task of image restoration [45]. In the current study, Hao et al. (2024) proposed the Dilated Strip Attention Network (DSAN) for restoring images with state-of-the-art performance in various picture restorative tasks with the ability to aggregate context information in images with multi-scale strip fields in both horizontal and vertical strips of images.

Because of the stability, consistency, and continuous utilization in current studies of medical image denoising, traditional methods such as DnCNN and Noise2Noise, announced in 2016 and 2018, respectively, are still widely used extensively as traditional benchmark comparisons. By adopting these models, it is feasible to make comparisons among the previous studies while focusing also on the relative progress of new architectures introduced more recently. With the aid of attention mechanisms, the proposed FUDA-NET model has always shown improvements over U-Net with a PSNR improvement of about 1.5-2.5 dB, while SSIM and FSIM improved equivalently. These improvements are attributed to enhanced structural preservation with reduced over-smoothing, observed in visualization comparisons, although improvements in PSNR alone are not adequate in clinical relevance. These improvements can play an important role in clinical settings for medical imaging because these improvements can ensure the easy visualization of diagnostically relevant information such as the shapes of tissues and boundaries of cells. More rigorous clinical validations are, however, argued to be essential in future studies.

### *7.4 Clinical Validation and Diagnostic Relevance*

While quantitative image quality criteria like PSNR, SSIM, and FSIM provide objective assessment of denoising performance, clinical application requires the preservation of diagnostically important features. Structures such as nuclear morphology, cellular borders, and tissue organization provide important clues for accurate diagnosis and grading in the context of histopathological imaging. In order to qualitatively judge therapeutic relevance, the denoised images produced by the proposed FUDA-NET were inspected visually, with particular attention being paid to the preservation of nuclear form, chromatin patterns, and cellular features. The results demonstrate that FUDA-NET removes noise without over-smoothing fine morphological features, thus avoiding the suppression of characteristics critical to diagnosis. In contrast, numerous baseline approaches either result in over-smoothing or residual noise, either of which might impair visual interpretability. Qualitative comparative visual assessments suggest that the proposed FUDA-NET preserves salient diagnostic cues more faithfully than the competitive methods, although there is no formal reader study involving expert pathology interpretation. These results propose that the proposed denoising framework as a preprocessing step towards histopathological image analysis could be applicable in real-world applications. In addition, the improvement of the quality of the denoising procedure by removing noise effects could have a profound effect on subsequent processes such as disease detection, staging, and analysis. The FUDA-Net model promises to give more accurate results to medical professionals and computer-aided systems through capturing structure without compromising clarity. The future work involves evaluating the entire clinical validation process.

## 8. Conclusion

In this research work, a new denoising framework, FUDA-NET (Fuzzy U-Net with Dual Attention), has been conceptualized and developed for high-quality denoising of noisy histopathological medical images. The proposed FUDA-NET model Integrates Multi stage U-Net Encoder-Decoder layers, Dual Attention (channel and spatial), and the fuzzy-logic based feature modulation layer for adaptive feature refinement and noise removal. Various experiments are performed on High Grade Serous Ovarian Cancer histopathological image dataset with 12,019 training and 1,188 testing images. The denoising efficacy of the FUDA-NET model has been compared with several State-of-The-Art techniques, namely DnCNN, U-Net, U-Net with Attention, and Noise2Noise. The outcome of this research work clearly illustrates the superiority of FUDA-NET through quantitative analysis relating to various parameters such as PSNR, SSIM, MSE, MAE, and FSIM. Of prime note is the fact that FUDA-NET has been able to measure the PSNR's existence of 35 decibels for all test sets, establishing a better image quality. Additionally, it has been observed that FUDA-NET indicates a reduced error rate with a higher structural and perception similarity measure, establishing its proficiency in retaining diagnostic characteristics for medical image preservation.

## References


[1] Moschetta, M., George, A., Kaye, S. B., & Banerjee, S. (2016). BRCA somatic mutations and epigenetic BRCA modifications in serous ovarian cancer. *Annals of Oncology*, *27*(8), 1449-1455.

[2] Stewart, C., Ralyea, C., & Lockwood, S. (2019, April). Ovarian cancer: an integrated review. In *Seminars in oncology nursing* (Vol. 35, No. 2, pp. 151-156). WB Saunders.

[3] Hamad, M. M., Aktar, S., Uddin, M. J., Rahman, T., Alyami, S. A., Al-Ashhab, S., & Moni, M. A. (2022). Early-stage detection of ovarian cancer based on clinical data using machine learning approaches. *Journal of Personalized Medicine*, *12*(8), 1211.

[4] Boehm, K. M., Aherne, E. A., Ellenson, L., Nikolovski, I., Alghamdi, M., Vázquez-García, I., & Shah, S. P. (2022). Multimodal data integration using machine learning improves risk stratification of high-grade serous ovarian cancer. *Nature Cancer, 3*(6), 723–733.

[5] Cho, H. W., Cho, H., Kim, J., Kim, S., Lee, S., Song, J. Y., & Lee, J. K. (2024). Pelvic ultrasound-based deep learning models for accurate diagnosis of ovarian cancer: Retrospective multicenter study.

[6] Farahani, H., Boschman, J., Farnell, D., Darbandsari, A., Zhang, A., Ahmadvand, P., & Bashashati, A. (2022). Deep learning-based histotype diagnosis of ovarian carcinoma whole-slide pathology images. *Modern Pathology, 35*(12), 1983–1990.

[7] Zhang, R., Siu, M. K., Ngan, H. Y., & Chan, K. K. (2022). Molecular biomarkers for the early detection of ovarian cancer. *International Journal of Molecular Sciences*, *23*(19), 12041.

[8] Zamwar, U. M., & Anjankar, A. P. (2022). Aetiology, epidemiology, histopathology, classification, detailed evaluation, and treatment of ovarian cancer. *Cureus*, *14*(10).

[9] Ghoniem, R. M., Algarni, A. D., Refky, B., & Ewees, A. A. (2021). Multi-modal evolutionary deep learning model for ovarian cancer diagnosis. *Symmetry, 13*(4), 643. https://doi.org/10.3390/sym13040643

[10] Guo, L. Y., Wu, A. H., Wang, Y. X., Zhang, L. P., Chai, H., & Liang, X. F. (2020). Deep learning-based ovarian cancer subtypes identification using multi-omics data. *BioData Mining, 13*, 1–12.

[11] Jung, Y., Kim, T., Han, M. R., Kim, S., Kim, G., Lee, S., & Choi, Y. J. (2022). Ovarian tumor diagnosis using deep convolutional neural networks and a denoising convolutional autoencoder. *Scientific Reports, 12*(1), 17024.

[12] Kim, M., Chen, C., Wang, P., Mulvey, J. J., Yang, Y., Wun, C., & Heller, D. A. (2022). Detection of ovarian cancer via the spectral fingerprinting of quantum-defect-modified carbon nanotubes in serum by machine learning. *Nature Biomedical Engineering, 6*(3), 267–275.

[13] Octaviani, T. L., Rustam, Z., & Siswantining, T. (2019, June). Ovarian cancer classification using Bayesian logistic regression. *IOP Conference Series: Materials Science and Engineering, 546*(5), 052049.

[14] Saida, T., Mori, K., Hoshiai, S., Sakai, M., Urushibara, A., Ishiguro, T., & Nakajima, T. (2022). Diagnosing ovarian cancer on MRI: A preliminary study comparing deep learning and radiologist assessments. *Cancers*, *14*(4), 987.

[15] Schwartz, D., Sawyer, T. W., Thurston, N., Barton, J., & Ditzler, G. (2022). Ovarian cancer detection using optical coherence tomography and convolutional neural networks. *Neural Computing and Applications*, *34*(11), 8977–8987.

[16] Jung, Y., Kim, T., Han, M. R., Kim, S., Kim, G., Lee, S., & Choi, Y. J. (2022). Ovarian tumor diagnosis using deep convolutional neural networks and a denoising convolutional autoencoder. *Scientific Reports*, *12*(1), 17024.

[17] Xu, X., Kapse, S., Gupta, R., & Prasanna, P. (2023, October). Vit-dae: Transformer-driven diffusion autoencoder for histopathology image analysis. In *International Conference on Medical Image Computing and Computer-Assisted Intervention* (pp. 66-76). Cham: Springer Nature Switzerland.

[18] Ghoniem, R. M., Algarni, A. D., Refky, B., & Ewees, A. A. (2021). Multi-modal evolutionary deep learning model for ovarian cancer diagnosis. *Symmetry*, *13*(4), 643.

[19] Sengupta, D., Ali, S. N., Bhattacharya, A., Mustafi, J., Mukhopadhyay, A., & Sengupta, K. (2022). A deep hybrid learning pipeline for accurate diagnosis of ovarian cancer based on nuclear morphology. *PloS one*, *17*(1), e0261181

[20] Chen, H., Yang, B. W., Qian, L., Meng, Y. S., Bai, X. H., Hong, X. W., ... & Feng, W. W. (2022). Deep learning prediction of ovarian malignancy at US compared with O-RADS and expert assessment. *Radiology*, *304*(1), 106-113

[21] Ziyambe, B., Yahya, A., Mushiri, T., Tariq, M. U., Abbas, Q., Babar, M., ... & Jabbar, S. (2023). A deep learning framework for the prediction and diagnosis of ovarian cancer in pre-and post-menopausal women. *Diagnostics*, *13*(10), 1703.

[22] Mohammed, M., Mwambi, H., Mboya, I. B., Elbashir, M. K., & Omolo, B. (2021). A stacking ensemble deep learning approach to cancer type classification based on TCGA data. *Scientific reports*, *11*(1), 15626.

[23] Huttunen, M. J., Hassan, A., McCloskey, C. W., Fasih, S., Upham, J., Vanderhyden, B. C., ... & Murugkar, S. (2018). Automated classification of multiphoton microscopy images of ovarian tissue using deep learning. *Journal of biomedical optics*, *23*(6), 066002-066002.

[24] Wu, M., Yan, C., Liu, H., & Liu, Q. (2018). Automatic classification of ovarian cancer types from cytological images using deep convolutional neural networks. *Bioscience reports*, *38*(3), BSR20180289.

[25] Gao, Y., Zeng, S., Xu, X., Li, H., Yao, S., Song, K., ... & Gao, Q. (2022). Deep learning-enabled pelvic ultrasound images for accurate diagnosis of ovarian cancer in China: a retrospective, multicentre, diagnostic study. *The Lancet Digital Health*, *4*(3), e179-e187.

[26] Adebayo, S. O., & Khan, A. H. (2025). Distributed Deep Learning for Medical Image Denoising with Data Obfuscation. 2025 IEEE 25th International Conference on Bioinformatics and Bioengineering (BIBE), 76–80. https://doi.org/10.1109/bibe66822.2025.00021

[27] Pfaff, L., Wagner, F., Vysotskaya, N., Thies, M., Maul, N., Mei, S., Wuerfl, T., & Maier, A. (2024). No-New-Denoiser: A Critical Analysis of Diffusion Models for Medical Image Denoising. Medical Image Computing and Computer Assisted Intervention – MICCAI 2024, 568–578. https://doi.org/10.1007/978-3-031-72117-5_53

[28] Ullah, F., Kumar, K., Rahim, T., Khan, J., & Jung, Y. (2025). A new hybrid image denoising algorithm using adaptive and modified decision-based filters for enhanced image quality. Scientific Reports, 15(1). https://doi.org/10.1038/s41598-025-92283-3

[29] Beibei, W. (2024). Research on denoising and enhancing methods of medical images based on convolutional neural networks. Concurrency and Computation: Practice and Experience, 36(11). Portico. https://doi.org/10.1002/cpe.8016

[30] Singh, P. (2025). Understanding Medical Image Denoising, Enhancement, and Reconstruction. Biomedical Informatics and Smart Healthcare, 1(1), 35-39.10.62762/BISH.2025.966762

[31] Wang, W., Xia, J., Luo, G., Dong, S., Li, X., Wen, J., & Li, S. (2025). Diffusion model for medical image denoising, reconstruction and translation. Computerized Medical Imaging and Graphics, 124, 102593. https://doi.org/10.1016/j.compmedimag.2025.102593

[32] https://www.kaggle.com/datasets/sunilthite/ovarian-cancer-classification-dataset

[33] Nivetha, S., & Inbarani, H. H. (2022). Neighborhood rough neural network approach for COVID-19 image classification. *Neural Processing Letters*, *54*(3), 1919-1941.

[34] Nivetha, S., & Inbarani, H. H. (2023). Novel Adaptive Histogram Binning-Based Lesion Segmentation for Discerning Severity in COVID-19 Chest CT Scan Images. *International Journal of Sociotechnology and Knowledge Development (IJSKD)*, *15*(1), 1-35.

[35] Nivetha, S., & Inbarani, H. H. (2023). Novel Hybrid Genetic Arithmetic Optimization for Feature Selection and Classification of Pulmonary Disease Images. *International Journal of Sociotechnology and Knowledge Development (IJSKD)*, *15*(1), 1-58.

[36] Nivetha, S., & Inbarani, H. H. (2023). Novel Architecture for Image Classification Based on Rough Set. *International Journal of Service Science, Management, Engineering, and Technology (IJSSMET)*, *14*(1), 1-38.

[37] Nivetha, S**.**, & Hannah Inbarani, H. (2022). Classification Of Covid-19 CT Scan Images Using Novel Tolerance Rough Set Approach. In *Machine Learning for Critical Internet of Medical Things: Applications and Use Cases* (pp. 55-80). Cham: Springer International Publishing.

[38] Nivetha, S., & Hannah Inbarani, H. (2022, September). Automated Lesion Image Segmentation Based on Novel Histogram-Based K-Means Clustering Using Covid-19 Chest CT Images organized by "Congress on Intelligent System (CIS 2022)" held on 05.09.2022 to 06.09.2022.
[39] Nivetha, S., Inbarani, H. H.: Novel Hybrid Genetic Arithmetic Optimization for Feature Selection and Classification of Pulmonary Disease Images. International Journal of Sociotechnology and Knowledge Development (IJSKD), 15(1), 1-58 (2023).
[40] Nivetha, S., & Hannah Inbarani, H.: Automated Histogram Binning-Based Fuzzy K-Means Clustering for COVID-19 Chest CT Image Segmentation. In: *Inventive Systems and Control: Proceedings of ICISC 2023*, pp. 777-793. Singapore: Springer Nature Singapore. (2023).
[41] Nivetha, S., Anandakumar, K., Inbarani, H. H., & Khan, M. (2025). Explainable machine learning framework for gene expression-based biomarker identification and cancer classification using feature selection. *Med. Data Min*, *8*(3), 19.
[42] Gautam, A., Pawar, A., Joshi, A., Tazi, S. N., Chaudhary, S., Hambarde, P., ... & Murala, S. (2025). Pureformer: Transformer-Based Image Denoising. In *Proceedings of the Computer Vision and Pattern Recognition Conference* (pp. 1441-1449).
[43] Tian, C., Zheng, M., Zuo, W., Zhang, S., Zhang, Y., & Lin, C. W. (2024). A cross transformer for image denoising. *Information Fusion*, *102*, 102043.
[44] Anwar, A., Shullar, M., Nasir, A. A., Masood, M., & Anwar, S. (2025). TDiR: Transformer based Diffusion for Image Restoration Tasks. *arXiv preprint arXiv:2506.20302*.
[45] Wu, Z., Chen, Y., Xiong, J., Pan, X., & He, W. (2025). S2TDM: Spatial-spectral transformer-based diffusion model for hyperspectral image denoising. *Geo-spatial Information Science*, 1-18.
[46] Hao, F., Wu, J., Du, J., Wang, Y., & Xu, J. (2024). Dilated Strip Attention Network for Image Restoration. *arXiv preprint arXiv:2407.18613*.

## Authors' Profiles

**K. Anandakumar** received his Master of Computer Applications (MCA) degree from Periyar University, Salem, India, in 2012. He is currently pursuing his Ph.D. as a Research Scholar in the Department of Computer Science at Periyar University, Salem, Tamil Nadu. His research interests include image processing, machine learning, and deep learning. He successfully cleared the State Eligibility Test (SET) in 2025.

**C. Chandrasekar** is a Senior Professor and Head in the Department of Computer Science at Periyar University, Salem, Tamil Nadu. He holds an M.C.A. and Ph.D., and has over 20 years of teaching and 15 years of research experience. He has completed funded projects with UGC, including a notable project on 4G mobile network mobility. Dr. C. Chandrasekar has published extensively in Scopus and SCI-indexed journals, and has represented his work internationally.

**How to cite this paper:** Anandakumar K., Chandrasekar C., "Fuzzy-Enhanced U-Net with Dual Attention for Histopathological Image Analysis in High Grade Serous Ovarian Cancer", International Journal of Image, Graphics and Signal Processing(IJIGSP), Vol.18, No.1, pp. 13-32, 2026. DOI:10.5815/ijigsp.2026.01.02